Research Article | Vol. 25, No. 3 | 6 Feb 2017 | OPTICS EXPRESS 2826

Optics EXPRESS

Transmitting more than 10 bit with a single photon

TRISTAN B. H. TENTRUP,[1,4] THOMAS HUMMEL,[1] TOM A. W. WOLTERINK, [1,2] RAVITEJ UPPU, [1] ALLARD P. MOSK, [1,3] AND PEPIJN W. H. PINKSE [1,5]

[1]*Complex Photonic Systems (COPS), MESA+ Institute for Nanotechnology, University of Twente, P.O. Box 217, 7500 AE Enschede, The Netherlands*
[2]*Laser Physics and Nonlinear Optics (LPNO), MESA+ Institute for Nanotechnology, University of Twente, P.O. Box 217, 7500 AE Enschede, The Netherlands*
[3]*Present address: Debye Institute for Nanomaterials Science, Utrecht University, PO Box 80000, Utrecht, The Netherlands*
[4]*t.b.h.tentrup@utwente.nl*
[5]*p.w.h.pinkse@utwente.nl*

Abstract: Encoding information in the position of single photons has no known limits, given infinite resources. Using a heralded single-photon source and a spatial light modulator (SLM), we steer single photons to specific positions in a virtual grid on a large-area spatially resolving photon-counting detector (ICCD). We experimentally demonstrate selective addressing any location (symbol) in a 9072 size grid (alphabet) to achieve 10.5 bit of mutual information per detected photon between the sender and receiver. Our results can be useful for very-high-dimensional quantum information processing.

OCIS codes: (270.0270) Quantum optics; (270.5565) Quantum communications; (110.7348) Wavefront encoding.

References and links

1. M. A. Nielsen and I. L. Chuang, *Quantum Computation and Quantum Information* (Cambridge University, 2010).
2. C. H. Bennett and G. Brassard, "Quantum cryptography: public key distribution and coin tossing," in "International Conference on Computers, Systems & Signal Processing, Bangalore, India, Dec 9-12, 1984," (1984), pp. 175–179.
3. W. K. Wootters and W. H. Zurek, "A single quantum cannot be cloned," Nature **299**, 802–803 (1982).
4. V. Scarani, H. Bechmann-Pasquinucci, N. J. Cerf, M. Dušek, N. Lütkenhaus, and M. Peev, "The security of practical quantum key distribution," Rev. Mod. Phys. **81**, 1301 (2009).
5. N. J. Cerf, M. Bourennane, A. Karlsson, and N. Gisin, "Security of quantum key distribution using d-level systems," Phys. Rev. Lett. **88**, 127902 (2002).
6. H. Bechmann-Pasquinucci and W. Tittel, "Quantum cryptography using larger alphabets," Phys. Rev. A **61**, 062308 (2000).
7. S. Gröblacher, T. Jennewein, A. Vaziri, G. Weihs, and A. Zeilinger, "Experimental quantum cryptography with qutrits," New J. Phys. **8**, 75 (2006).
8. M. Mirhosseini, O. S. Magaña-Loaiza, M. N. O'Sullivan, B. Rodenburg, M. Malik, M. P. J. Lavery, M. J. Padgett, D. J. Gauthier, and R. W. Boyd, "High-dimensional quantum cryptography with twisted light," New J. Phys. **17**, 033033 (2015).
9. M. Mafu, A. Dudley, S. Goyal, D. Giovannini, M. McLaren, M. J. Padgett, T. Konrad, F. Petruccione, N. Lütkenhaus, and A. Forbes, "Higher-dimensional orbital-angular-momentum-based quantum key distribution with mutually unbiased bases," Phys. Rev. A **88**, 032305 (2013).
10. N. Gisin, G. Ribody, W. Tittel, and H. Zbinden, "Quantum cryptography," Rev. Mod. Phys. **74**, 145 (2002).
11. I. Ali-Khan, C. J. Broadbent, and J. C. Howell, "Large-alphabet quantum key distribution using energy-time entangled bipartite states," Phys. Rev. Lett. **98**, 060503 (2007).
12. T. Zhong, H. Zhou, R. D. Horansky, C. Lee, V. B. Verma, A. E. Lita, A. Restelli, J. C. Bienfang, R. P. Mirin, T. Gerrits, "Photon-efficient quantum key distribution using time–energy entanglement with high-dimensional encoding," New J. Phys. **17**, 022002 (2015).
13. S. P. Walborn, D. S. Lemelle, M. P. Almeida, and P. H. S. Ribeiro, "Quantum key distribution with higher-order alphabets using spatially encoded qudits," Phys. Rev. Lett. **96**, 090501 (2006).
14. S. P. Walborn, D. S. Lemelle, D. S. Tasca, and P. H. S. Ribeiro, "Schemes for quantum key distribution with higher-order alphabets using single-photon fractional fourier optics," Phys. Rev. A **77**, 062323 (2008).

#281843 https://doi.org/10.1364/OE.25.002826
Journal © 2017 Received 8 Dec 2016; revised 13 Jan 2017; accepted 15 Jan 2017; published 2 Feb 2017

Optics EXPRESS

15. P. B. Dixon, G. A. Howland, J. Schneeloch, and J. C. Howell, "Quantum mutual information capacity for high-dimensional entangled states," Phys. Rev. Lett. **108**, 143603 (2012).
16. J. Wang, J-Y. Yang, I. M. Fazal, N. Ahmed, Y. Yan, H. Huang, Y. Ren, Y. Yue, S. Dolinar, M. Tur, and A. E. Willner, "Terabit free-space data transmission employing orbital angular momentum multiplexing," Nat. Photon. **6**, 488-496 (2012).
17. N. Zhao, X. Li, G. Li, and J. M. Kahn, "Capacity limits of spatially multiplexed free-space communication," Nat. Photonics **9**, 822–826 (2015).
18. J. M. Kahn, G. Li, X. Li, and N. Zhao, "To twist or not to twist: capacity limits of free-space channels," in "Advanced Photonics 2016 (IPR, NOMA, Sensors, Networks, SPPCom, SOF)" (2016), SpM4E.1
19. D. J. Gauthier, C. F. Wildfeuer, H. StipÄĐeviÄĞ, B. Christensen, D. Kumor, P. Kwiat, K. McCusker, T. Brougham, and S. M. Barnett, "Quantum key distribution using hyperentangled time-bin states," in "Proceedings of The Tenth Rochester Conference on Coherence on Quantum Optics (CQO10)," (2014), pp. 234–239.
20. D. J. C. MacKay, *Information Theory, Inference and Learning Algorithms* (Cambridge University, 2003).
21. R. Gallager, "Low-density parity-check codes," IRE Trans. Inf. Theory **8**, 21–28 (1962).
22. F. Gray, "Pulse code communication," US Patent 2,632,058 issued March 17 (1953).
23. T. Čižmár and K. Dholakia, "Shaping the light transmission through a multimode optical fibre: complex transformation analysis and applications in biophotonics," Opt. Express **19**, 18871–18884 (2011).
24. L. V. Amitonova, A. P. Mosk, and P. W. H. Pinkse, "Rotational memory effect of a multimode fiber," Opt. Express **23**, 20569–20575 (2015).
25. D. J. Lum, J. C. Howell, M. S. Allman, T. Gerrits, V. B. Verma, S. W. Nam, C. Lupo, and S. Lloyd, "Quantum enigma machine: experimentally demonstrating quantum data locking," Phys. Rev. A **94**, 022315 (2016).
26. D. P. DiVincenzo, M. Horodecki, D. W. Leung, J. A. Smolin, and B. M. Terhal, "Locking classical correlations in quantum states," Phys. Rev. Lett. **92**, 067902 (2004).
27. T. A. W. Wolterink, R. Uppu, G. Ctistis, W. L. Vos, K.-J. Boller, and P. W. H. Pinkse, "Programmable two-photon quantum interference in 10^3 channels in opaque scattering media," Phys. Rev. A **93**, 053817 (2016).
28. B. Jost, A. Sergienko, A. Abouraddy, B. Saleh, and M. Teich, "Spatial correlations of spontaneously down-converted photon pairs detected with a single-photon-sensitive ccd camera," Opt. Express **3**, 81–88 (1998).
29. A. F. Abouraddy, M. B. Nasr, B. E. A. Saleh, A. V. Sergienko, and M. C. Teich, "Demonstration of the complementarity of one-and two-photon interference," Phys. Rev. A **63**, 063803 (2001).
30. O. Jedrkiewicz, Y.-K. Jiang, E. Brambilla, A. Gatti, M. Bache, L. Lugiato, and P. Di Trapani, "Detection of sub-shot-noise spatial correlation in high-gain parametric down conversion," Phys. Rev. Lett. **93**, 243601 (2004).
31. O. Haderka, J. Peřina Jr, M. Hamar, and J. Peřina, "Direct measurement and reconstruction of nonclassical features of twin beams generated in spontaneous parametric down-conversion," Phys. Rev. A **71**, 033815 (2005).
32. H. D. L. Pires, C. H. Monken, and M. P. van Exter, "Direct measurement of transverse-mode entanglement in two-photon states," Phys. Rev. A **80**, 022307 (2009).
33. R. S. Aspden, D. S. Tasca, R. W. Boyd, and M. J. Padgett, "Epr-based ghost imaging using a single-photon-sensitive camera," New J. Phys. **15**, 073032 (2013).
34. R. Fickler, M. Krenn, R. Lapkiewicz, S. Ramelow, and A. Zeilinger, "Real-time imaging of quantum entanglement," Sci. Rep. **3**, 1914 (2013).
35. R. Chrapkiewicz, W. Wasilewski, and K. Banaszek, "High-fidelity resolved multiphoton counting for quantum imaging applications," Opt. Lett. **39**, 5090-5093 (2014).
36. I. M. Vellekoop and A. P. Mosk, "Focusing coherent light through opaque strongly scattering media," Opt. Lett. **32**, 2309–2311 (2007).

1. Introduction

Its weak interaction with the environment makes light ideal for sharing information between distant parties. For this reason, light is used to transmit information all around the world. With the advent of single-photon sources, a new class of applications has emerged. Due to their quantum properties, single photons are used to entangle quantum systems or to do quantum cryptography [1]. One famous example is Quantum Key Distribution (QKD) using the BB84 protocol [2] to securely build up a secret shared key between Alice and Bob. The security of this method is based on the no-cloning theorem [3], which forbids copying quantum states. The standard implementation of the BB84 protocol uses the two-dimensional polarization basis to encode information in photons. Therefore the alphabet contains only two symbols "0" and "1", limiting the information content per photon to 1 bit. Increasing the dimension of the basis using a large alphabet increases the information content per photon together with an improvement in the security [4–6]. This is the motivation to employ larger alphabets using orbital angular momentum [7–9], time binning [10–12] or spatial translation [13–15]. Among

Optics EXPRESS

the spatial encoding schemes, Orbital Angular Momentum (OAM) states have been proposed for high-dimensional information encoding [16]. However in a practical scenario, assuming a sender-receiver configuration with apertures of finite size, a diffraction-limited spot translated in space or Laguerre-Gauss modes has a higher capacity limit than the subset of pure OAM states [17, 18]. This makes spatial positioning of light or equivalently, tilting of plane waves, an ideal method for increasing the information content per photon. Interestingly, given infinite resources, there is no known upper bound for the information content transmitted by single photons. For example, using one mole $\left(6.022 \cdot 10^{23}\right)$ of ideal position-sensitive single-photon detectors leads to an information content of 79 bit per detected photon. Clearly, this is out of reach in a practical situation. A very relevant question therefore is what can be realised experimentally.

In this article we report our experiment in which we have deterministically encoded more than 10 bit of information into a single photon. We have employed 2^3 times more symbols than previous work in spatial encoding, which reported 7 bit per photon as highest value for random keys [15], and is comparable to what has been achieved in temporal and polarization encoding [19].

2. Result

The spatial encoding of information is realized on a rectangular, virtual grid formed by binning the pixels of a camera. The experimental setup is schematized in Fig. 1 and details are given in Methods. In case the entire camera chip would be used, the maximum information is $\log_2(1024 \cdot 1024) = 20$ bit. If we fill in our experimental parameters, namely a signal-to-dark-count ratio of 10.08 and a focus size of 8 pixels in each direction on the ICCD, this number is reduced to 14.45 bit. In our experiment we used a grid of 112×81 areas of binned pixels, which are the 9072 symbols of our alphabet. This value corresponds to a maximum information content of $\log_2(9072) = 13.15$ bit.

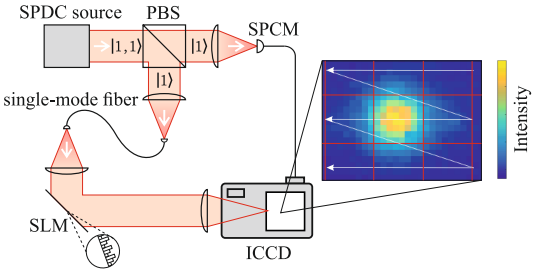

Fig. 1. Schematic representation of the setup. The Type-II Spontaneous Parametric Down-Conversion (SPDC) source produces photon pairs, which are split by a Polarising Beam Splitter (PBS). One of the photons is detected by a Single-Photon Counting Module (SPCM) acting as a herald for an Intensified CCD (ICCD). The other photon is fiber-coupled and is incident on a Spatial Light Modulator (SLM). Its Fourier image is projected on the ICCD. The position of the focus is scanned by adjusting the blazed grating on the SLM, indicated by the arrows. An accumulated focus is shown in a zoom-in of the ICCD image integrated over an average of 1000 photons. The red lines show the 8×8 pixel binning of the symbols.

The light is directed to distinct symbols on the grid by scanning the focus using a SLM as a blazed grating. We assume that the sender uses an alphabet X and the receiver an alphabet Y. To characterize the system, we sample the joint probability distribution $P(X, Y)$, which indicates the probabilities $p(x, y)$ to detect a certain symbol y out of the alphabet Y if a symbol x out of the alphabet X was sent. The result is plotted in Fig. 2. The readout noise of the ICCD was reduced by applying a threshold on the measured signal to only show the intensified signal. A diagonal line in the plot of the sent symbol versus the received would indicate maximal correlation. Indeed

Optics EXPRESS

there is a strong correlation between the sent and received symbol set visible in graph (a), which shows the whole alphabet in a log-log plot. Graph (b) depicts a zoom into the first 200 of the 9072 symbols. Due to crosstalk between the symbols, off-diagonal lines are visible, which correspond to photons hitting the symbol above or below the target. The distance of 112 symbols between these lines and the diagonal corresponds to the column length of the grid written on the camera. The signal to the left and right of the diagonal is caused by crosstalk to the left and right symbol on the grid. Noise can also arise from dark counts of the ICCD.

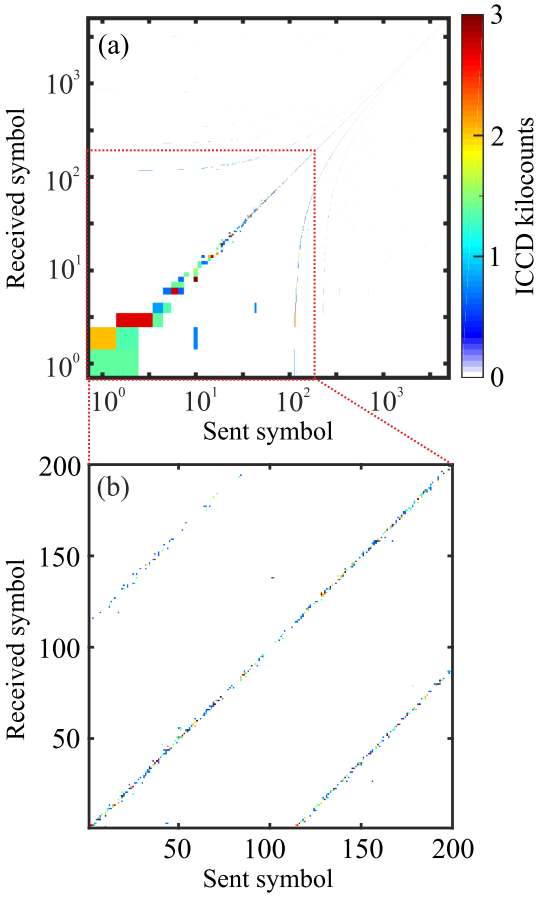

Fig. 2. Measured ICCD counts in each of the measured symbols as a function of the sent symbol with a binning size of 8 × 8 pixels. The exposure time was 0.6 s for each symbol. Graph (a) illustrates the correlation between all 9072 symbols in a log-log plot. The graph (b) shows the measured correlation between the first 200 symbols in a linear plot. The measurement samples the joint probability distribution $P(X, Y)$.

To quantify the information content per photon, we calculate the mutual information between sender and receiver. The mutual information $I(X : Y)$ is the measure of the average reduction in uncertainty about a sent symbol set X that results from learning the value of the received symbol set Y; or vice versa, the average amount of information that X conveys about Y [20]. The mutual information per detection event of the sender-receiver system is mathematically represented as

$$I(X : Y) = \sum_{x \in X, y \in Y} p(x, y) \log_2 \left(\frac{p(x, y)}{p(x)p(y)} \right), \tag{1}$$

Optics EXPRESS

where $p(x, y)$ is the probability that symbol y is received when symbol x is sent. $p(y)$ is the probability to measure symbol y and $p(x)$ the probability that the sender encodes the symbol x. Theoretically, the mutual information depends on the number of symbols N, which has a maximum of $I_{\max} = \log_2(N)$, assuming $p(x) = 1/N$ for every symbol $x \in X$. In the experiment, we ensured the uniform probability of x to realize the theoretical maximum in the absence of noise. The maximum number of symbols is limited by the finite size of the CCD. Using the presented binning size of the detection areas of 8×8, our theoretical limit is 13.15 bit.

In reality, the mutual information is not only limited by the number of symbols and the entropy of the sent alphabet, but also reduced by the crosstalk between the symbols arising from diffraction-limited focal spots as well as the noise from environment and detector. In order to reduce the crosstalk between the symbols, the binning size of the detection areas can be increased. This, however, reduces the number of symbols given the limited number of pixels on the detector. The blue circles in Fig. 3 show the dependence of the maximum mutual information for symbols made with different pixel bin sizes. The measured mutual information for 8×8 and 12×12 pixel bin sizes are represented as red circles. The measured data is lower than the theoretical limit. This can be understood from the average hit probability, indicated by the green + markers. Moreover, accounting for a finite signal-to-dark-photocount ratio between 10 and 100, leads to the expected mutual information, depicted as gray bars in the figure. As evident from the figure, there is a maximal mutual information given by physical limitations of crosstalk and noise. For large bin sizes with near-zero crosstalk between symbols, one can achieve very high mutual information of over 9 bit per photon. Given the FWHM spot size of approximately 8 pixels, we choose an 8×8 binning achieving a value of 10.5 bit of mutual information per detected photon.

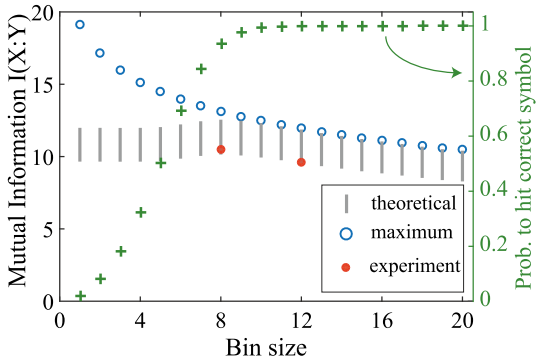

Fig. 3. Dependence of the mutual information and the average hit probability in the correct symbol on the binning size of the detection areas. The blue circles represent the theoretical limit $I_{\max}$ given no noise or crosstalk. The red dots correspond to the measured mutual information for 8×8 and 12×12 pixel bin size. The theoretical mutual information is shown as gray bars in the figure, corrected for a signal-to-dark-count photon ratio between 10 and 100. The green + markers illustrate the average hit probability in the correct area for a finite focal diameter with FWHM of 8 pixels as shown in Fig. 1.

To calculate the mutual information per *sent* photon, one has to take the losses in our setup into account. This includes the coupling losses into the single mode fibres of 55%, the diffraction losses at the SLM of 24%, the losses at the spectral filter of 30% and the losses at the detector due to the limited quantum efficiency of 5%. This leads to a channel capacity of 0.1 bit per photon.

Optics EXPRESS

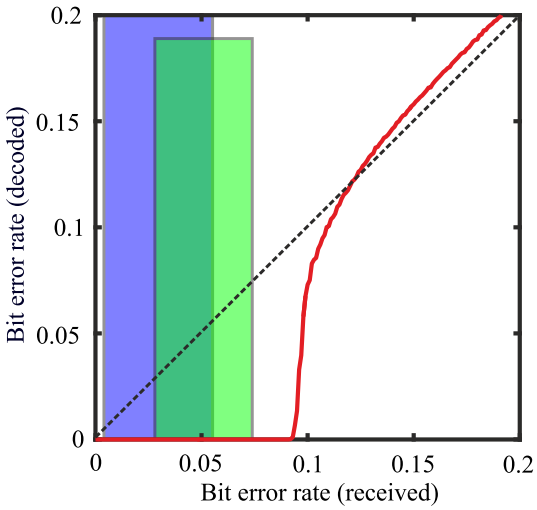

Fig. 4. The Bit Error Rate (BER) of the received bit string versus the BER of the bit string after performing error correction. The dashed diagonal line represents the result without error correction. The vertical bars indicate the estimated BER of our experiment in case of 8×8 (green) and 12×12 (blue) binning. Their left and right edges indicate a signal-to-dark-count photon ratio of 100 and 10, respectively.

3. Discussion and summary

For useful communication, the errors within the received message have to be corrected. An efficient way of error correction is the Low-Density Parity-Check Code (LDPC) [21]. In order to apply this error correction, all symbols of the set have to be translated into a bit string. Therefore we encode the x and y position of our symbols independently, each allocating half the bits. Since the dominant noise term is the crosstalk between the neighbouring symbols, we use a Gray code [22] for each direction. This causes only one bit flip for an erroneous detection by a neighbouring symbol either in x or the y direction.

Figure 4 shows the Bit Error Rate (BER) after error correction with LDPC versus the BER of the received bit string. The LDPC code was set to the half-rate LDPC used in digital television broadcast standard DVB-S.2. The coloured vertical bars indicate the estimated BER in case of 8×8 and 12×12 binning. The estimation takes the measured crosstalk between the symbols into account. Their left and right edges indicate a signal-to-dark-count photon ratio of 100 and 10, respectively. For the ICCD used in these measurements, this ratio is 10.07. Other commercially available ICCD have ratios close to 100, explaining the choice of the other bound. Clearly, already a standard error-correction code allows a practically error-free communication with the present system.

In conclusion, we demonstrate high-dimensional encoding of single photons reaching 10.5 bit per photon. The capacity of this spatial encoding is only limited by the optics and the number of pixels on the detector. The channel capacity of 0.1 bit can be increased by reducing the losses in the system. The main contribution to losses in our setup arises from the low quantum efficiency ($\sim 5\%$) of the ICCD, which can be improved to $\sim 30\%$ with different photocathode materials. This makes it possible to reach a signal-to-dark-count ratio of 100 and would bring the measured values closer to its theoretical maximum. Our results are directly applicable to free-space line-of-sight communication. If the scrambling of wavefronts in multimode fibers can be controlled [23, 24], a second and potentially more robust carrier for this high-dimensional encoding can be realised. A very promising direction for this work would then be the implementation of a

Optics EXPRESS

large-spatial-alphabet encoding for quantum key distribution or high-dimensional quantum data locking [25, 26].

4. Methods

4.1. Setup

The setup is illustrated in Fig. 1. We use a Spontaneous Parametric Down-Conversion source [27] to produce photon pairs. A 790 nm mode-locked picosecond laser with a pulse repetition rate of 76 MHz is frequency doubled to 395 nm in a LBO crystal. The frequency-doubled light is focussed in a Periodically Poled Potassium Titanyl Phosphate (PPKTP) crystal, which spontaneously produces orthogonally polarized photon pairs at a wavelength of 790 nm. The entangled photon pair is separated at a Polarizing Beam Splitter into two single-photon Fock states. One of these photons is sent to a Single Photon Counting Module acting as a herald, while the second photon is directed through a 28.5 m single-mode fiber with a throughput of 47% to the encoding setup. For free-space communication, one needs an encoding device at the sender position and a decoding device on the receiver position. As encoding device we use a phase-only Spatial Light Modulator to modulate the wavefront of the single photons. By writing a blazed grating on the SLM, we change the reflection angle within an angular range of 0.8° in vertical and horizontal direction with a diffraction efficiency of 76% in the first order. The Fourier transform of the SLM is imaged with a 1 m focal length lens in 2f configuration onto a large-area spatially resolving photon-counting detector. A bandpass filter at 800 ± 40 nm is placed in front of the detector to block stray light.

4.2. Detector

The decoding device should be able to measure the arrival of a single photon in a single shot on a large area. One technology that can achieve this is the Intensified Charge-Coupled Device [28–35]. ICCDs provide nanosecond gating option, which reduces the amount of dark counts significantly and makes such an ICCD capable of heralded measurements, reducing dark counts to one per thousands of readouts. The dark counts of the ICCD have their origin in thermal electrons released by the photocathode of the ICCD. Additionally, residual gas atoms can be ionized by the electron avalanche within the Microchannel Plate (MCP) of the intensifier. These ions are accelerated towards the photocathode by the MCP bias voltage, releasing secondary electron avalanches. An ion impact causes many more electrons than an incoming photon does. This leads to a local signal increase on the ICCD camera which is brighter than the signal produced by a single photon. Therefore these spurious ion signals can be filtered out in postprocessing. Our model (Andor iStar A-DH334T-18u-A3) has a photocathode quantum efficiency of 5%. Each heralded photon from the SPDC source opens the ICCD gate for 2 ns. For the measurements in Fig. 2 6 images with an exposure time of 0.1 s have been taken at each symbol. Single photon events were analyzed using threshold photon counting [35], with the threshold level set above the readout noise of the CCD camera. Attenuating the SPDC to a herald rate of ∼ 400 kHz, we measured on average 7.3 photon detections per symbol. The FWHM of the focus, with a constant phase pattern on the SLM and integrated over an average of 1000 photon detection events, was found to be 7.9 ± 0.3 pixels horizontally and 7.4 ± 0.2 pixels vertically.

4.3. Encoding

The target position of the photon on the ICCD is determined by the horizontal and vertical diffraction angle of the grating on the SLM. Although a scan mirror could be used for spatial encoding, a SLM is a more flexible tool. Via holography, the phase and amplitude of a wavefront can be manipulated, allowing to use complex wavefronts. Moreover, the path of the light can be corrected for disturbances using wavefront-shaping methods [36]. The SLM (pixel pitch: 20 μm,

Optics EXPRESS

resolution: 800x600 pixels) is programmed with horizontal and vertical gratings to scan over the detection plane of the ICCD. The angular range of encoded alphabets is small ($\sim 0.33^o$) and the grating pitch was over 5 pixels, which ensured high and uniform diffraction efficiency for all symbols. In order to define the sent symbol, the position on the ICCD has to be mapped to separate symbols. For this reason, a grid is defined on the ICCD. The pixels of the ICCD are binned together in detection areas of 8×8 or 12×12 pixels, forming an alphabet of 9072 or 4050 symbols, respectively. This rectangular map on the detection plane of the ICCD connects every detection area to an individual label, numbered from left to right and top to bottom.

Funding

European Research Council (ERC) (279248); Stichting voor Fundamenteel Onderzoek der Materie (FOM); Nederlandse Organisatie voor Wetenschappelijk Onderzoek (NWO).

Acknowledgments

We would like to thank Klaus Boller, Boris Škorić and Willem Vos for support and discussions. We also like to thank Daniel Gauthier for making us aware of reference [19].